Molecular Vision 2005; 11:1122-34 <http://www.molvis.org/molvis/v11/a130/>
Received 27 April 2005 | Accepted 8 December 2005 | Published 15 December 2005

Examining the proteins of functional retinal lipofuscin using proteomic analysis as a guide for understanding its origin

Sarah Warburton,[1] Katie Southwick,[1,2] Ryan M. Hardman,[1] Aaron M. Secrest,[1] Ryan K. Grow,[1] Huijun Xin,[1] Adam T. Woolley,[1] Gregory F. Burton,[1] Craig D. Thulin[1,2]

[1]Department of Chemistry and Biochemistry, and the [2]Proteomics and Biological Mass Spectrometry Facility, Brigham Young University, Provo, UT

Purpose: To elucidate the origins of biologically active retinal lipofuscin (RLF) by examining its protein composition.
Methods: Total protein and total lipid were extracted and quantified. Proteins in this lipoprotein granule were identified by limited-scale proteomic analysis using both two-dimensional (2D) gel electrophoresis and SDS-PAGE coupled with MALDI-QqToF MSMS and automated LCMSMS, respectively.
Results: RLF granules were 44% protein and 50% lipid. Proteomic analyses identified 41 constituent proteins. Hydrophobic proteins and several proteins specific to photoreceptors, including rhodopsin, that have not previously been reported, were identified. Extensive protein modification, especially oxidative damage, was observed.
Conclusions: Proteins identified support the model that RLF accumulates in RPE cells as a result of the buildup of undigested material from the phagocytosis of photoreceptor outer segments. Perhaps oxidative damage renders some of these proteins indigestible and thus leads to the accumulation of RLF granules.

Several retinal diseases including age-related macular degeneration (AMD), Stargardt's disease, and Best's macular dystrophy result from the degeneration of cells in the retina. These diseases have also been associated with the accumulation of autofluorescent lipofuscin granules in the retinal pigment epithelium (RPE) [1,2]. Many tissues accumulate lipofuscin granules, also called age pigments, but the retinal lipofuscin (RLF) that accumulates in RPE cells is probably unique. RPE cells are reported to begin accumulating RLF granules around age 20; and by age 80 these granules may constitute up to 20% of the cell volume [3]. RLF may relate to the onset of these ocular diseases because it has been shown to generate reactive oxygen species via photosensitization with blue light [4-7], which may cause damage and death of the RPE and surrounding cells.

RLF is known to be a heterogeneous material composed of a mixture of proteins and lipids, including several different fluorescent compounds. More than ten different fluorophores from RLF have been observed by thin layer chromatography [8,9] but the only fully characterized fluorophore is the bisretinoid, A2E [10]. One would expect to find an abundance of hydrophobic and highly modified, microheterogenous, proteins in RLF granules because of their lipophilic nature and the inability of RPE cells to degrade them. Recently another publication reported the identification of proteins in RLF granules using two-dimensional (2D) gel electrophoresis [11]. Due to the limitations of 2D electrophoresis including the lack of solubility of hydrophobic proteins in buffer systems compatible with 2D gel electrophoresis, and the inability to focus microheterogeneous proteins into observable spots, this method may limit the proteins amenable to identification.

The origin of RLF has not been completely established, but the granules are thought to result from the accumulation of undigested material from the phagocytosis of photoreceptor discs in RPE lysosomes. The material is thought to be undegradable by the cell, perhaps because of modifications that inhibit degradation. Knowledge of the composition and origin of lipofuscin granules could be useful for designing therapies to prevent lipofuscin accumulation and the onset of AMD. Elucidating the protein constituents of RLF could provide significant insight into the origin of these granules.

In this study we employed both one-dimensional (1D) and 2D gel electrophoresis to provide a view of the proteins in RLF, and demonstrated the presence of modifications on these proteins. Our results are compared to a recent publication [11] reporting the identification of proteins in RLF granules in which only 2D electrophoresis was employed. Our findings provide strong evidence for the model that retinal lipofuscin results from an accumulation of undigested material from the phagocytosis of photoreceptor discs in RPE lysosomes, and also suggest a possible mechanism for the inhibition of phagosomal/lysosomal digestion.

METHODS

Lipofuscin isolation and fluorescence: Lipofuscin granules were isolated from human RPE from donor eyes, provided by Dr. Paul Bernstein of the Moran Eye Institute, (University of Utah, Salt Lake City, UT). We use RPE from human donor eyes provided by the Utah Lions Eye Bank, after they have been released for research use. Any unused tissue is returned to the Eye Bank for proper disposal. No identifying informa-

Correspondence to: Craig D. Thulin, Department of Chemistry and Biochemistry, Benson Building, Room C-100, Brigham Young University, Provo, UT, 84602; Phone: (801) 422-2795; FAX: (801) 422-0153; email: craig_thulin@byu.edu

tion beyond age, gender, brief ocular history, and cause of death is supplied to our laboratory. All specimens are accepted without regard to gender, race, or ethnic origin. No formal human subjects approval is required by the University for research studies on donated human tissue (E4 exemption). The time between donor death and enucleation was 1-4 h after which the donor eyes were stored at 4 °C until dissection. Dissections were carried out 6-24 h after donor death in a dim light environment by Dr. Bernstein's lab at the Moran Eye Institute. RPE's were shipped to BYU on dry ice and stored at -75 °C until use. RPE's from twenty randomly selected individuals between 20 and 80 years of age, were used for each preparation of isolated lipofuscin. The lipofuscin granules were isolated using a sucrose gradient as described by Boulton et al. [12]. Fluorescence spectra of isolated lipofuscin granules were acquired as described by Boulton et al. [12] using a Jobin Yvon Fluoromax-3 Spectrofluorometer (Edison, NJ).

Bioactivity assay: ARPE-19 (human retinal pigment epithelial cells-ATCC-CRL-2302) were grown in 96 well tissue culture plates and were maintained in RPMI 1640 media supplemented with 10% fetal bovine serum (FBS). Cells were differentiated by transferring them to Matrigel Basement Membrane Matrix (BD Biosciences, Bedford, MA) and reducing the FBS in the media to 1% for two weeks. Upon differentiation, cells were either maintained in RPMI 1640 media supplemented with 1% FBS or incubated in the same media which also contained about 90 lipofuscin granules/cell for 24 h to allow for ingestion of the granules. After the 24 h incubation, the lipofuscin-fed RPE cells were transferred back to RPMI 1640 media supplemented with 1% FBS and maintained for 7 days before use in bioactivity assay. To verify the bioactivity of the RLF, differentiated ARPE-19 cells that were fed RLF or maintained as control cells were either subjected to blue light (390-550 nm) for 24-48 h at an intensity of about 2.8 mW/cm or maintained in the dark. Blue light was introduced into a humidified cell incubator using a Mille Luce M1000 Fiber Optic Illuminator with a 150 W quartz halogen bulb, a 25 mm dichroic blue light filter, and a 48 inch fiber optic cable (Edmund Optics, Barrington, NJ). Photocytotoxicity of the lipofuscin granules was assessed using the MTT Colorimetric Assay (Chemicon International, Temecula, CA). MTT (3-(4,5-dimehtylthiazol-2-yl)-2,5-diphenyl tetrasodium bromide) in PBS (pH 7.4) was added to each well and then incubated at 37 °C for 4 h. After incubation, developing solution containing 0.04 N HCl in isopropanol was added to each well and the absorbance was read at 570 nm on a CERES UV900 HDi plate reading spectrophotometer (Bio-Tek Instruments).

Microscopy: RLF granules were prepared for scanning electron microscopy (SEM) analysis by drying the granules on a silicon wafer and sputter coating them with gold. The granules were analyzed on a Phillips XL30 ESEM FEG using a 5 kV accelerating potential. For transmission electron microscopy (TEM) analysis RLF granules were fixed in glutaraldehyde, postfixed in osmic acid, dehydrated, and embedded in epoxy resin. Slices of the sample (100 nm) were imaged and photographed on a JEOL JEM 2000 FX. RLF samples for atomic force microscopy (AFM) were prepared by drying the granules onto a mica slide. Images were taken with a Multimode IIIa AFM instrument with microfabricated Si cantilever tips (Nanoscience Instruments, Phoenix, AZ). Vibrational noise was dampened using an active isolation system (MOD1-M, Halcyonics, Goettingen, Germany). Typical imaging parameters were: tip resonance frequency, 55-65 kHz; amplitude setpoint, 2.0-2.5 V; scan rate, 2.0 Hz. Images were processed offline to remove the background slope using software bundled with the AFM instrument.

Total lipid determination in lipofuscin: Lipofuscin granules were collected by centrifugation and dried in an evaporative centrifugal concentrator. The granules were weighed using a Mettler UMT2 microbalance (Columbus, OH) to determine the total mass of the granules. After weighing the dried granules, lipids in lipofuscin samples were extracted in chloroform:methanol (2:1, v/v). The lipid extract was dried in an evaporative centrifugal concentrator and weighed using the microbalance to determine the total mass of lipids.

Total protein determination in lipofuscin: After weighing samples of lipofuscin granules as above, the protein in these lipofuscin samples was quantified by solubilizing 150 μg of lipofuscin protein (about 380 μg lipofucin) in 30 μl of 1% (w/v) SDS followed by the BCA Protein Assay (Pierce, Rockford, IL).

2D Gels: RLF granules containing 300 μg of protein were collected by centrifugation at 6000x g and solubilized in reswelling buffer (7 M urea, 2 M thiourea, 15 mM dithiothreitol (DTT), and 1% pharmalites) with either 4% Triton X-100 or 0.5% Triton X-100 and 2% ASB-14 (Calbiochem, San Diego, CA). Both cuploading and reswelling procedures were used to analyze the proteins. Isoelectric focusing was performed using a 7 cm immobilized pH gradient (IPG) pH 4-7 on a Multiphor II Electrophoresis System (Amersham Pharmacia Biotech, Piscataway, NJ). A programmed voltage gradient was used consisting of 200 V for 1 min, linearly increasing to 3500 V over 1.5 h, and held at 3500 V for 1.5 h to reach a total of approximately 8 kVh. Following isoelectric focusing, IPG strips were washed in equilibration buffer (0.05 M Tris, 6 M urea, 30% glycerol, and 1% SDS) containing 32 mM dithiothreitol for 15 min followed by a 15 min wash in equilibration buffer containing 216 mM iodoacetamide. The proteins were then separated according to their molecular weight on a 10% gel (8.3x6.4x0.1 cm) using standard SDS-PAGE conditions. Gels were stained with colloidal coomassie (Pierce), and were analyzed using Melanie 4 software (GeneBio, Geneva, Switzerland [13]). Internal pI and molecular weight standards were used to assist in alignment of gels. Excised spots were trypsinized in-gel [14], desalted using a $ZipTip_{U\text{-}C18}$ (Millipore, Bedford, MA), and analyzed by oMALDI Qq-ToF (orthogonal matrix-assisted laser desorption ionization quadrupole time-of-flight) mass spectrometry on an Applied Biosystems QSTAR Pulsar i instrument (Foster City, CA). Sample spots of 1 μl were allowed to co-crystallize on the MALDI plate with 1 μl of α-cyano 4-hydroxycinnamic acid as the matrix.

1D Gel and mass spectrometry: Lipofuscin granules containing 100 μg of protein were collected by centrifugation,

solubilized in 20 µl 4X Laemmli buffer (3% SDS, 0.17 M Tris pH 6.8, 35% glycerol, 3.5% 2-mercaptoethanol) and separated on a 10% SDS-polyacrylamide gel (8.3x6.4x0.1 cm). The proteins were in-gel digested as described by Shevchenko et al. [14], injected onto a Jupiter C18 reversed-phase resin capillary column (150 µm IDx20 cm, made in-house) and eluted using a gradient of 5 to 95% acetonitrile in 0.1% formic acid at a flow rate of 5 µl/min. On-line mass spectrometric analysis was performed on an Applied Biosystems QSTAR Pulsar i using an atmospheric pressure ionization (API) source. Automated tandem mass spectrometry using information-dependent acquisition was run, collecting collision induced dissociation (CID) spectra for the three most intense ions from each survey scan excluding peaks chosen in the preceding 2 min. Fragmentation spectra were chosen by hand for submission to the Mascot (Matrix Science) website for peptide identification. The ProID extension of BioAnalyst (Applied Biosystems, Foster City, CA) was also used to identify modifications on RLF proteins.

Immunoelectron microscopy: Granules were collected by centrifugation and fixed with either 2% glutaraldehyde or 2% paraformaldehyde. The granule pellets were dehydrated in ethanol and embedded in LR White resin, one of the most infiltratable resins specifically designed for immunocytochemical techniques. Slices of the samples (100 nm) were collected on formvar-coated gold grids. Grids were incubated first in 4% bovine serum albumin (BSA) for 15 min at room temperature to block nonspecific binding sites, then in either a 1:1000 dilution of anti-rhodopsin IgG (R4, polyclonal antibody Takemoto et al. [15]) or anti-phosducin IgG [16] (negative control) overnight at 4 °C, and finally a 1:100 dilution of anti-rabbit IgG gold-conjugate (10 nm, Sigma, St. Louis, MO) for 2 h at 37 °C. Between each incubation period the grids were washed four times for 2 min each in either Tris Buffer A pH 8.2 (200 mM NaCl, 20 mM Tris, 1% NP40, 0.05% Tween 20) or Tris Buffer B pH 8.2 (200 mM NaCl, 20 mM Tris). The grids were stained with uranyl acetate and lead citrate prior to examining them on a FEI Tecnai 12 (Hillsborough, OR) transmission electron microscope. Micrographs from two samples were used in the analysis, one sample was fixed with paraformaldehyde and washed with Tris Buffer A and the other sample was fixed with glutaraldehyde and washed with Tris Buffer B. Because fixation of the sample requires alteration of protein constituents, this process can block or impede antigen labeling. Therefore, different fixation procedures were explored to ensure appropriate labeling of the sample. The gold particles, associated with the RLF granules and the resin (nonspecific binding), in the micrographs were counted in a total area of about 120 µm^2 containing about 100 granules. Adobe Photoshop was used to determine the area occupied by granules and resin in the micrographs. The area occupied by granules and resin was normalized to half of the total area. That normalization was applied to the gold particle count to accurately determine the fraction of gold particles bound to RLF granules.

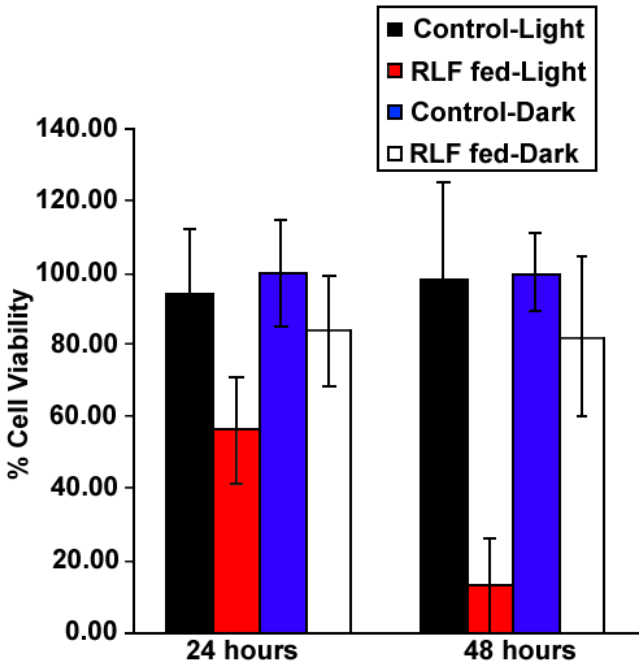

Figure 1. Bioactivity of RLF granules. Isolated RLF granules were fed to differentiated ARPE-19 cells which were then allowed to recover for 7 days. Cells that were not fed RLF were used as controls. Cells were then subjected to blue light irradiation (black or red), or left in the dark (blue or white), for 24-48 h as described in the text. Cell viability was determined using the MTT assay. Values represent means of 8-12 independent measurements, error bars representing standard deviation. The light dependent cell death of arpe-19 cells fed RLF granules indicates that our RLF is biologically active.

Flow cytometric analysis: To determine the size distribution and concentration (granules/unit volume), suspensions of RLF granules were diluted 1:100, and 1:1000 with PBS, and 200,000 Flow Check High Intensity Green Alignment Beads (Polysciences, Inc., Warrington, PA), 5.726±0.375 µm in diameter, were added to each sample to serve as an internal standard. The samples were excited with an argon laser at 488 nm on a Beckman Coulter (Beckman, Fullerton, CA) EPICS-XL Flow Cytometer with EXPO 32 ADC software for flow cytometric analysis. The samples were analyzed for light scatter and autofluorescence by collection of data for 300 s, which allowed visualization of at least 5,000 beads and at least 49,000 RLF granules.

Immunoblots: Human retinas were obtained from Dr. Paul Bernstein from the Moran Eye Institute to provide a positive control for rhodopsin. A retina was gently triturated in 0.75 M sucrose, 0.68 mM $CaCl_2$, 20 mM Tris and 1 mM DTT, pH 7.4 to rupture the cells. The suspension was poured over 4 thicknesses of cheesecloth to remove cellular debris. The sample was centrifuged at 1475x g for 20 min and the pellet was resuspended in 1% SDS. Total protein was determined using the BCA assay.

Anti-rhodopsin antibody (R4) was used at 1:1000 dilution in Tris buffered saline with 0.05% (w/v) Tween (TBS-T). Anti-CRALBP antibody (Dr. John C. Saari, University of Washington, Seattle, WA) was used at a 1:1000 dilution in TBS-T. RLF protein (30 µg) was separated on a 1D gel and

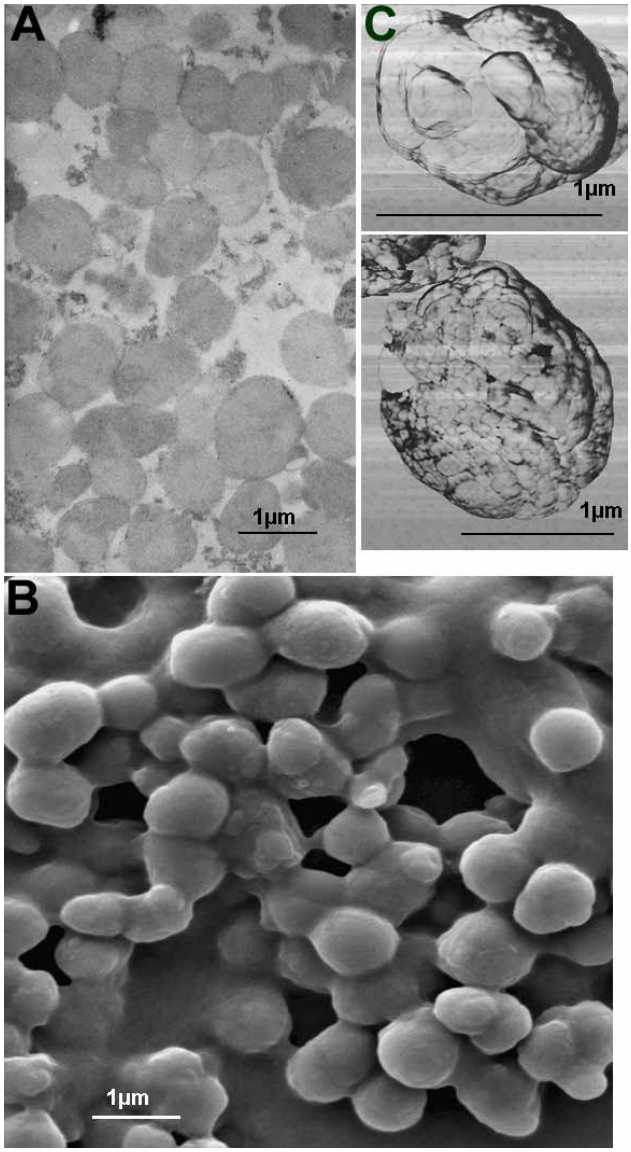

Figure 2. Microscopy of RLF granules. **A**: Transmission electron micrograph of RLF, showing granules of homogeneous density. **B**: Scanning electron micrograph of RLF, showing nearly spherical granules with some surface features. **C**: Atomic force micrographs (phase images) showing RLF granules to be aggregates of about 200 nm (upper panel) and about 50 nm (both panels) substructures. AFM images were processed offline to remove the background slope using software bundled with the AFM instrument. Then granule size was more quantitatively determined using flow cytometric analysis (FC). Forward light scatter in FC instruments is directly proportional to the size of the objects passing through the beam. The RLF granules were found to be distributed into two populations by size, one (representing 99% of the granules) having a mean diameter of 0.69 µm with a Gaussian distribution and a broad standard deviation of 0.63 µm, and the other population (representing only 1% of the granules) having a mean diameter of 4.8 µm with standard deviation of 0.3 µm. The larger granules are not melanosomes because their fluorescence properties (measured by flow cytometry) match RLF, not melanosomes. Flow cytometry also enabled a quantitative determination of the concentration of granules in our suspensions. Having a quantitative count of the RLF granules we were able to determine their average weight, which proved to be 1.3±0.2 pg/granule.

analyzed for malondialdehyde (MDA)-modified proteins using a rabbit antibody to MDA (Calbiochem, San Diego, CA) diluted 1:1000 in TBS-T.

Oxidized BSA standards were made by incubating BSA in hypochlorous acid at 37 °C for 30 min. RLF and BSA samples were derivatized by incubating them in 5% sodium dodecyl sulfate and 10 mM 2,4-dinitrophenylhydrazine (DNP) in 10% (v/v) trifluoroacetic acid for 30 min at room temperature [17]. Laemmli buffer and 2 M Tris base was added to the samples until they turned from yellow to blue, indicating that the pH was neutral, before loading the samples onto a gel. Anti-DNP antibody from rabbit was used at a 1:1000 dilution (Sigma, St. Louis, MO).

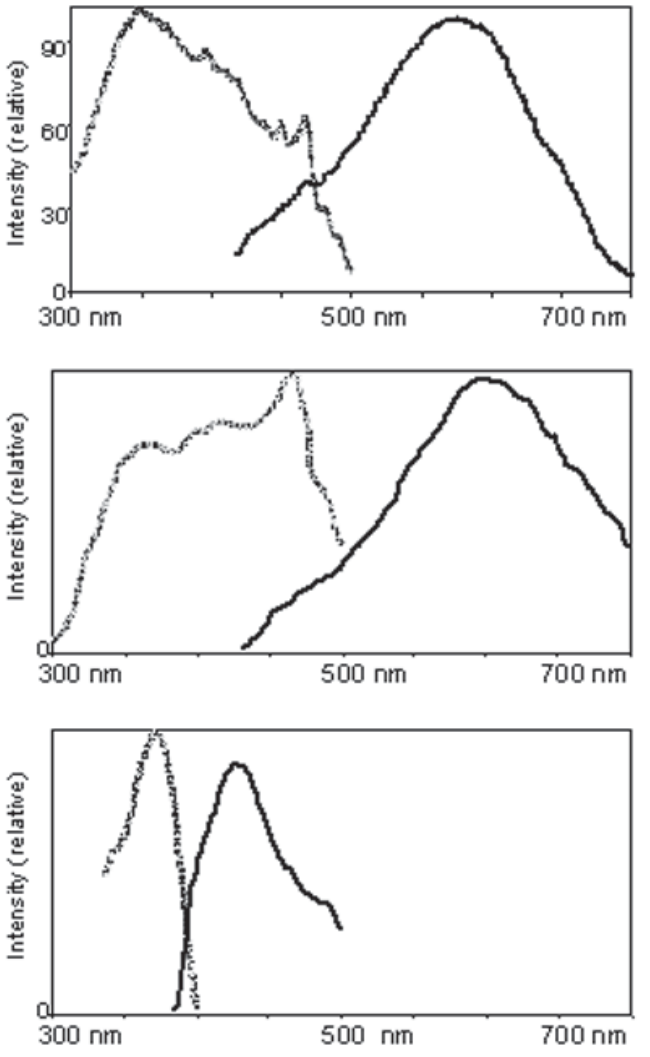

Figure 3. Fluorescence of RLF granules. Fluorescence spectroscopy of RLF from our preparations (top panel) compared with RLF from Boulton et al. [12] (middle panel) and Schutt et al. [11] (lower panel). The spectra from their published papers were simply traced. Excitation (gray) monitored with emission at 570 nm, and emission (black) monitored with excitation at 364 nm. Our evidence that supports the congruence of our preparations with those studied by Boulton et al. [12].

RESULTS

RLF granules, isolated as previously described [12], were found to be biologically active in retinal pigment epithelial (RPE) cells in culture (Figure 1). Several physical measurements of RLF granules were made, including electron microscopy, atomic force microscopy, and size distribution using flow cytometric analysis (Figure 2). Fluorescence spectra from our RLF preparations (Figure 3, top panel) showed extensive similarity to those published by Boulton et al. [12] (Figure 3, middle panel), with a broad excitation maximum between 350 and 450 nm and a broad emission maximum near 600 nm. Figure 3 also shows a comparison to excitation and emission spectra recently reported from Schutt et al. [11], which show a narrow excitation peak at 350 nm and a narrow emission peak at 450 nm.

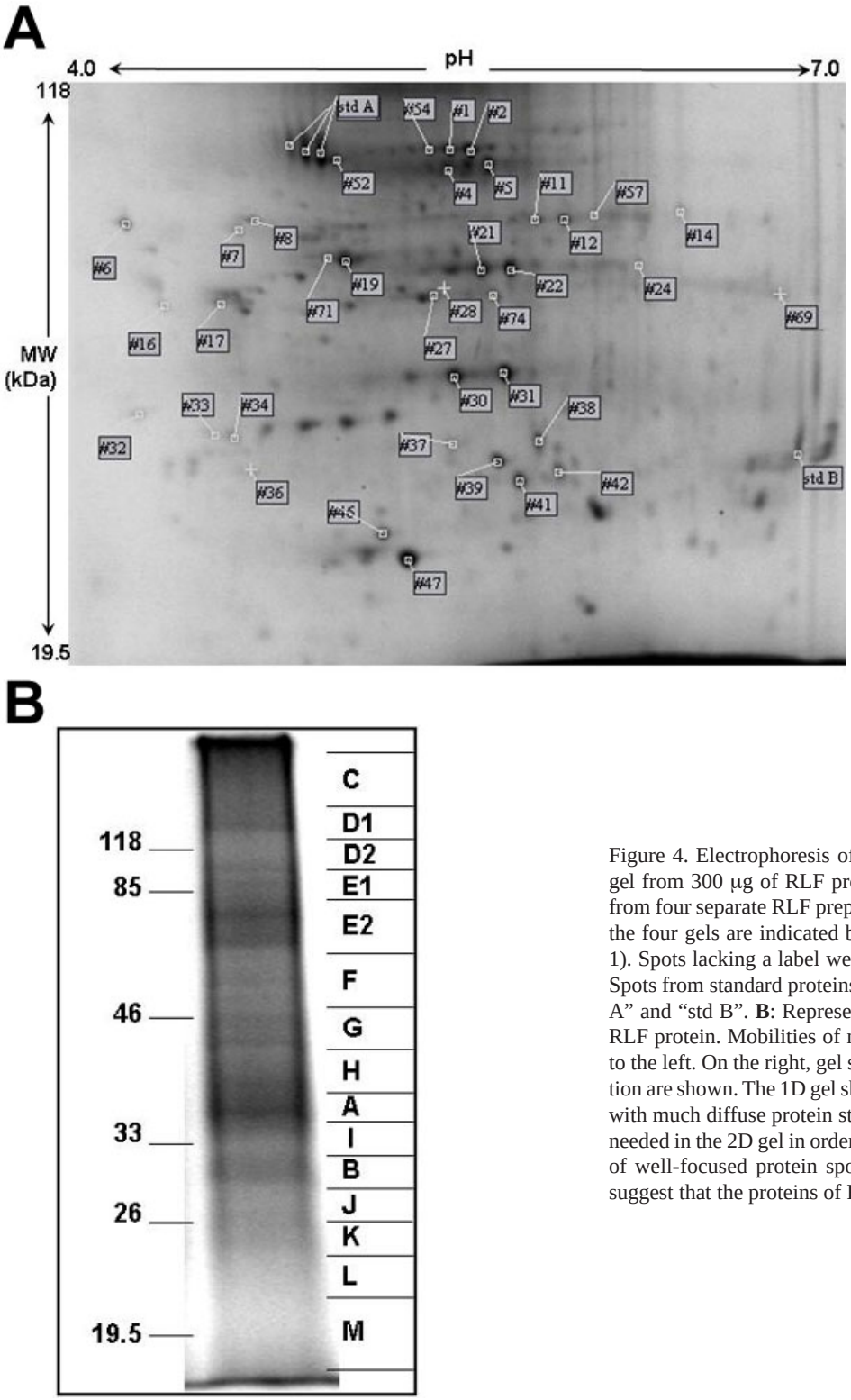

Figure 4. Electrophoresis of RLF proteins. **A**: 2D electrophoresis gel from 300 μg of RLF protein. This gel is representative of gels from four separate RLF preparations. Spots found in at least three of the four gels are indicated by their identifying spot number (Table 1). Spots lacking a label were unique to this particular preparation. Spots from standard proteins used to align gels are indicated as "std A" and "std B". **B**: Representative lane of SDS-PAGE of 50 μg of RLF protein. Mobilities of molecular weight markers are indicated to the left. On the right, gel slices taken for subsequent in-gel digestion are shown. The 1D gel shows relatively few well-resolved bands with much diffuse protein staining; thus 6 fold more total protein is needed in the 2D gel in order to observe a surprisingly small number of well-focused protein spots. Taken together, these observations suggest that the proteins of RLF are notably heterogeneous.

Transmission and scanning electron microscopy (TEM and SEM) as well as atomic force microscopy (AFM) were employed to examine the structure of RLF. TEM (Figure 2B) shows granules of approximately 0.7 μm in diameter of fairly uniform density, as has been previously reported [8,18,19]. Despite this apparent uniform density and rather simple circular cross-section, SEM (Figure 2C) shows that these granules are mostly spherical but appear to have some globular surface features that suggest aggregation. The aggregate nature of RLF is best illustrated by AFM. Figure 2D shows AFM phase images of two granules. In one (top panel), surface globules of about 200 nm diameter, noted in SEM, are seen and would seem to suggest growth by accretion. In both this picture and the other AFM view (Figure 2D lower panel), RLF appears to be made of smaller (about 50 nm) structures that are aggregated together. Taken together, the microscopic analyses show RLF granules to be composed of smaller structures of fairly uniform density that have accreted together to form the granules themselves. Granule size was more quantitatively determined using flow cytometric analysis (FC). Forward light scatter in FC instruments is directly proportional to the size of the objects passing through the beam. The RLF granules were found to be distributed into two populations by size, one (representing 99% of the granules) having a mean diameter of 0.69 μnm with a Gaussian distribution and a broad standard deviation of 0.63 μm, and the other population (representing only 1% of the granules) having a mean diameter of 4.8 μm with standard deviation of 0.3 μm. Flow cytometry also enabled a quantitative determination of the concentration of granules in our suspensions. Having a quantitative count of the RLF granules we were able to determine their average weight, which proved to be 1.3±0.2 pg/granule.

To determine the composition of the granules, first the lipids from a weighed quantity of granules were extracted in

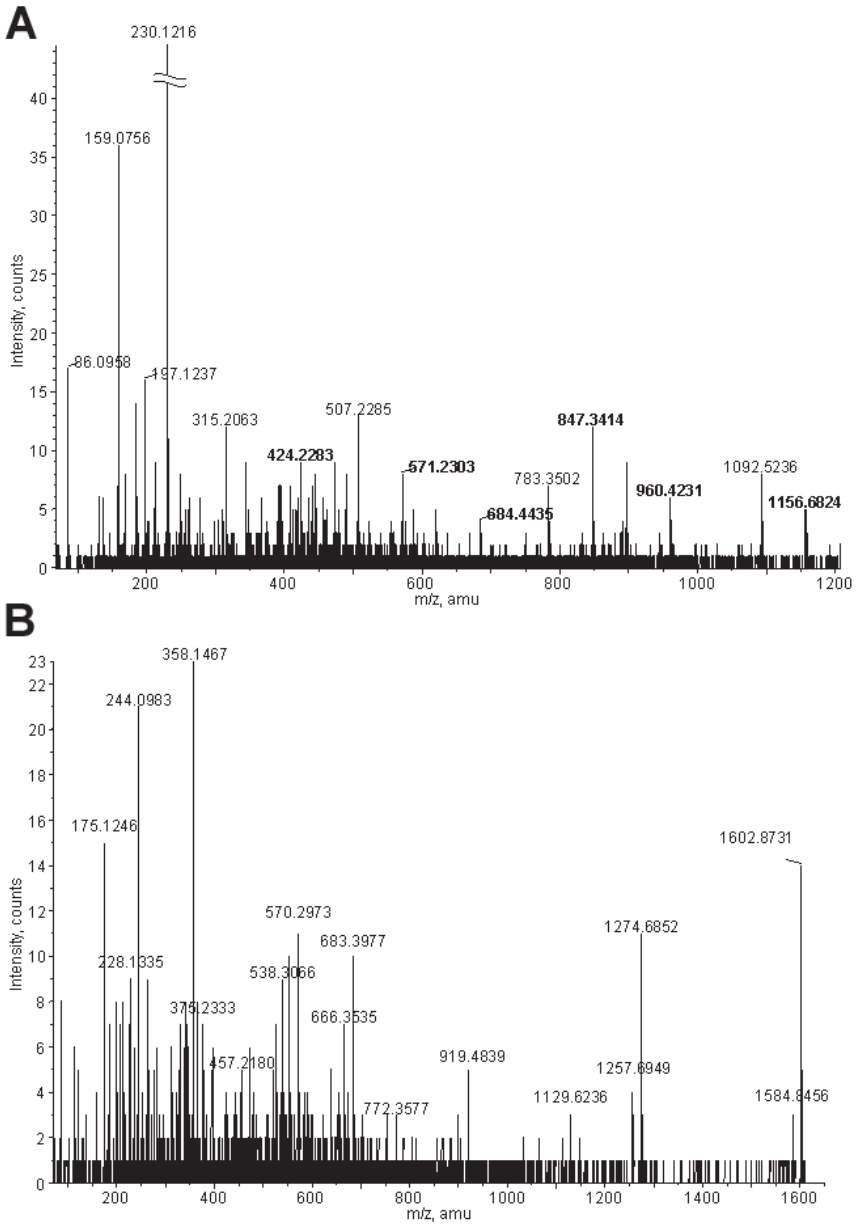

Figure 5. Mass spectrometry of peptides from RLF proteins. **A**: CID spectrum from LCMSMS of the peptide identified as SAAIYNPVIYIMO2MONK (where MO represents Met sulfoxide and MO2 represents Met sulfone) from rhodopsin. Indicated in bold are six y ions that make identification of these modified sites unequivocal. Another spectrum showed the same peptide with Met sulfoxide at the first Met position, and a third spectrum showed Met sulfone at the first Met without Met sulfoxide at the second Met position (data not shown). **B**: Representative CID spectrum from oMALDI MSMS. This peptide was identified as LVDQNIFSFYLSR from cathepsin D. The spectrum in **A** allows the conclusive identification of the modified methionines at positions 308 and 309 of rhodopsin. These spectra show that the fragmentation data obtained by both LCMSMS and oMALDI MSMS are of sufficiently high quality to allow unambiguous identification of the corresponding peptides.

TABLE 1. PROTEINS IDENTIFIED IN RETINAL LIPOFUSCIN

Protein	NCBI	Gel area/ spot number	Tissue specificity	Subcellular location	Alternate names	Gene ontology
1D gel system						
4F2 antigen heavy chain	177207	D2		type II membrane protein	CD98 antigen	calcium ion/amino acid transport
11-cis retinol dehydrogenase	2492753	I	retinal pigment epithelium	membrane-associated	retinol dehydrogenase	visual perception
acyl-CoA dehydrogenase	3273228	F		mitochondrial inner membrane		fatty acid beta-oxidation
alpha 1-antitrypsin	24438	H	plasma	extracellular	alpha-1-antiproteinase	endopeptidase inhibitor activity
alpha-tubulin 4	32015	A, D2				protein binding
alpha-tubulin 1*	37492	F				protein binding
anion transport protein	28714	D1	erythrocytes	integral membrane protein	AE 1, CD233 antigen	cell ion homeostasis
annexin A2*	18645167	A		membrane associated	lipocortin II	calcium ion binding
beta-globin*	29446	B	erythrocytes		hemoglobin beta chain	oxygen transport activity
calnexin	2134858	E1		type I membrane protein		calcium ion binding
cathepsin D*	494296	B		lysosomal		lysosome
ceroid-lipofuscinosis	5729770	H		lysosomal	tripeptidyl-peptidase I	tripeptidyl-peptidase I
cytochrome c oxidase II subunit	14016	L		integral membrane protein, mitochondrial inner membrane	cytochrome c oxidase	cytochrome-c oxidase activity
interphotoreceptor retinoid-binding protein	33961	D1	interphotoreceptor matrix		interstitial retinol-binding protein	lipid metabolism, visual peception
keratin	30154839	B, F, M				cytoskeleton organization
lysosomal integral membrane protein II	1362856	E1		type II membrane protein, lysosomal	LIMP II, CD36 antigen like 2	integral to plasma membrane
myelin protein zero	127721	A, B, D1/2, E1/2, F, I, J, L	peripheral nervous system schwann cells	type I membrane protein		structural molecule activity, synaptic transmission
NADH-ubiquinone oxidoreductase	128826	E1		mitrochondrial inner membrane	NADH dehydrogenase	electron carrier activity
Na+/K+-exchanging ATPase	88214	D1		integral membrane protein	sodium pump 3	ATP hydrolysis, proton transport
peripherin	4506465	A	photoreceptor rod rim region	integral membrane protein	retinal degeneration slow protein	visual perception
phospholipase C-alpha	303618	F		endoplasmic reticulum	protein disulfide isomerase A3	signal transduction
rhodopsin	4506527	D1/2, E1/2, F, G, H, I	photoreceptor rod	integral membrane protein	Opsin 2	phototransduction, G-protein coupled receptor activity
rod outer segment membrane protein I	4506575	A, D2, H, I	photoreceptor rod rim region	integral membrane protein	ROSP1	visual perception
retinal pigment epithelium-specific protein	4506591	D2, E1/2	retinal pigment epithelium		RPE65	visual perception
retinal S-antigen*	4506781	F, G	retina and pineal gland		rod photoreceptor arrestin	signal transduction
serum albumin*	28592	A	plasma	secreted		body fluid osmoregulation
transducin	31865	A	photoreceptor rod	membrane associated		visual perception
trypsin	136429	A, D1/2, E1/2, F, G, H, I, M		extracellular		protease
2D gel system						
ATP synthase, beta subunit*	32189394	19, 47, 71		mitochondria, membrane protein		tranpsorter activity
calnexin	2134858	3		type I membrane protein, ER		calcium ion binding
calreticulin*	4757900	6		endoplasmic reticulum lumen		protein folding
calumenin	2809324	16	ubiquitously expressed	endoplasmic retic. lumen/secreted	crocalbin	calcium ion binding
creatine kinase/ arginine kinase*#	180570	74		cytoplasmic		creatine kinase activity
cathepsin D*	494296	37,38		lysosomal		
ceroid-lipofuscinosis, neuronal 2	5729770	21,24		lysosomal		
dnaK-type molecular chaperone HSPA5	87528	4,5,52		endoplasmic reticulum lumen		
heat shock protein gp96a	15010550	7		endoplasmic reticulum lumen	GRP94, tumor rejection antigen	response to unfolded protein
KIAA0908	4240305	57	ubiquitous	lysosomal	prenylcysteine oxidase	lysosome, lyase activity
KIAA0617	40788303	30	widely expressed	nuclear and golgi		cell cycle arrest
motor protein*	516764	74		mitochondrial inner membrane	mito. inner memb. protein, mitofilin	mitochondrial inner membrane
mutant β-actin	28336	27		cytoplasmic		acetyltransferase complex
NADH-ubiquinone oxidoreductase	128826	1, 2, 32, 33, 41, 54		mitrochondrial inner membrane	NADH dehydrogenase	electron carrier activity

TABLE 1, CONTINUED.

Protein	NCBI	Gel area/ spot number	Tissue specificity	Subcellular location	Alternate names	Gene ontology
phospholipase c-α	303618	11		endoplasmic reticulum		signal transduction
pre-mRNA splicing factor SF2p32	338043	32		mitochondrial matrix	hyaluronan-binding protein 1	immune response
prohibitin*	4505773	39	widely expressed	cytoplasmic		regulation of cell cycle
protein disulfide isomerase	5031973	7,12,19		endoplasmic reticulum lumen		
vimentin*	4507895	17		highly expressed in fibroblasts		structural constituent

These proteins were identified from in-gel digestion followed by mass spectrometry from the respective SDS-PAGE gel regions or 2D gel spots. These proteins demonstrate that RLF contains components of photoreceptor disks and of lysosomes. Furthermore, 1D- and 2D-based protein identification is complementary, with 1D-based methods identifying significantly more of the heterogeneous and hydrophobic proteins that are found in RLF. We could not differentiate between creatine kinase and arginine kinase because of identical peptide sequences. KIAA0617 was only identified from one peptide with relatively low confidence. Items marked with an asterisk (*) were previosly reported in Schutt et al. [11].

methanol:chloroform, transferred, evaporated to dryness and weighed. This revealed that RLF was 49.5%±1.1% extractable lipid by weight. These percentages represent the mean of three independent measurements and indicate the standard deviation. Next, the protein in a known quantity of RLF was solubilized in 1% SDS and quantified by BCA assay. RLF consisted of 43.5%±2.6% total protein. Thus, these granules were composed nearly entirely of lipid and protein. These percentages represent the mean of three independent measurements and indicate the standard deviation.

In order to analyze the protein component of RLF, the granules were subjected to 2D gel electrophoresis. Initial attempts yielded very few protein spots. Only after loading significantly more protein (300 μg) than would typically be needed to examine an entire cell extract (about 100 μg total protein) were significant numbers of spots visible (Figure 4A).

2D gel electrophoresis of RLF proteins using a common isoelectric focusing buffer that contained 4% Triton X-100 resulted in 37% fewer spots than when the same sample was run in buffer with 0.5% Triton X-100 and 2% ASB-14 (data not shown). ASB-14 is a zwitterionic detergent known to facilitate the entry of transmembrane and other hydrophobic proteins into 2D gels [20]. The results reported were obtained using ASB-14 in the reswelling buffer.

2D gels were run analyzing proteins from four independent preparations of RLF granules. These gels showed some variation in number of spots, ranging from 53 to 121 (with an average of 78.5 spots per gel). The image processing program Melanie 4 was used to compare and match spots from the different gels. A "synthetic gel" was constructed in silico using this software, where each spot in the synthetic gel represented a spot present in at least three of the four 2D gels. Forty-four spots were found in the synthetic gel, including the five internal pI standards that had been added before electrophoresis. Nineteen proteins were identified from the 2D gels, correspond to "37 of the 39 spots (some proteins run as more than one spot due to posttranslational modifications)".

Because of the limitations of 2D electrophoresis, we also analyzed RLF proteins that had been solubilized in 1% SDS using 1D SDS-PAGE (Figure 4B). The overall pattern of bands seen in Figure 4B was qualitatively reproducible from one preparation of RLF granules to another. Regions of the 1D gel were cut out and trypsinized for subsequent analysis and protein identification using HPLC with on-line ESI-QqToF tandem mass spectrometry (LCMSMS) techniques (Figure 5A). These protein identifications were compared with those for proteins from spots in the 2D gels, which were excised, trypsinized, and identified using MALDI-QqToF mass spectrometry (Figure 5B).

Twenty-seven proteins were identified in 1D gel regions (Table 1), including five that were also found in the 2D spots. Thus, 22 proteins were identified in 1D gel regions that were not identified in the 2D gels. Notably, though 27 proteins were identified, many good quality CID spectra (defined as spectra that have at least four fragment peaks of signal:noise >5 between 500 and 1300 m/z) did not yield credible protein identification.

Among the proteins identified in 1D gel regions but not in the 2D gels was rhodopsin. Because of its importance and abundance in the photoreceptor cells which are phagocytosed by the RPE, we examined the rhodopsin in RLF further. Figure 6 shows immunoblot analyses of both 1D and 2D separations of RLF proteins, probed with an antibody raised against rhodopsin. In both of these blots, the microheterogeneity of the rhodopsin population in RLF was evident. The 2D immunoblot explains why no rhodopsin was identified from the 2D gel, since no well-focused spots were observed. This is despite the apparent abundance of RLF rhodopsin, based on the 1D immunoblot. Some of the modification responsible for the observed heterogeneity of RLF rhodopsin was determined to be oxidative damage. The tryptic peptide containing Met308 and Met309 was found by mass spectrometry bearing one, two, and three extra oxygen atoms which MSMS localized to the tripeptide IMM, residues 307-309 of rhodopsin, indicating oxidation of one or both of these Met residues to the Met sulfoxide or even the Met sulfone (Figure 5A). Rhodopsin was further confirmed to be a component of RLF granules by immunocytochemistry. Electron micrographs of RLF showed gold-conjugated protein A bound to anti-rhodopsin antibodies on the RLF granules (Figure 7). Over two-thirds of the gold

particles in these micrographs were found on RLF granules when corrections were made for the total area within and between granules.

Another protein of significant interest was the cellular retinoid binding protein CRALBP, which can be used as a molecular marker for RPE cells [21]. CRALBP was not identified in 1D gel slices of RLF proteins, but was identified by mass spectrometry from a lower abundance spot seen in one of the four 2D gels. 1D immunoblots showed that while CRALBP was present in RLF protein extracts, it was not very abundant (Figure 8).

In light of the oxidation seen on rhodopsin, and in view of the hypothesis that oxidative damage may be involved in the generation of RLF, we examined the RLF proteins for oxidative modifications using DNP, which derivatizes protein carbonyls [22]. Figure 9A shows an immunoblot of DNP-derivatized RLF proteins using an anti-DNP antibody which binds to the hydrazones formed by derivatization of the oxidatively formed carbonyls. Additional immunoblots revealed RLF proteins containing lipid peroxidation- or glucoxidation-induced damage, specifically malondialdehyde (MDA, Figure 9B), and advanced glycation end products (AGE), respectively. Protein oxidation was seen to be extensive (proteins across the molecular weight range of the 1D gel were seen to be modified) in the anti-DNP immunoblot. Notably, no well-focused spots of DNP-labeled proteins were detected in 2D immunoblots (data not shown). This suggests that many proteins that were oxidatively damaged were too heterogeneous to be observed in 2D gels, and therefore cannot be identified using this kind of separation.

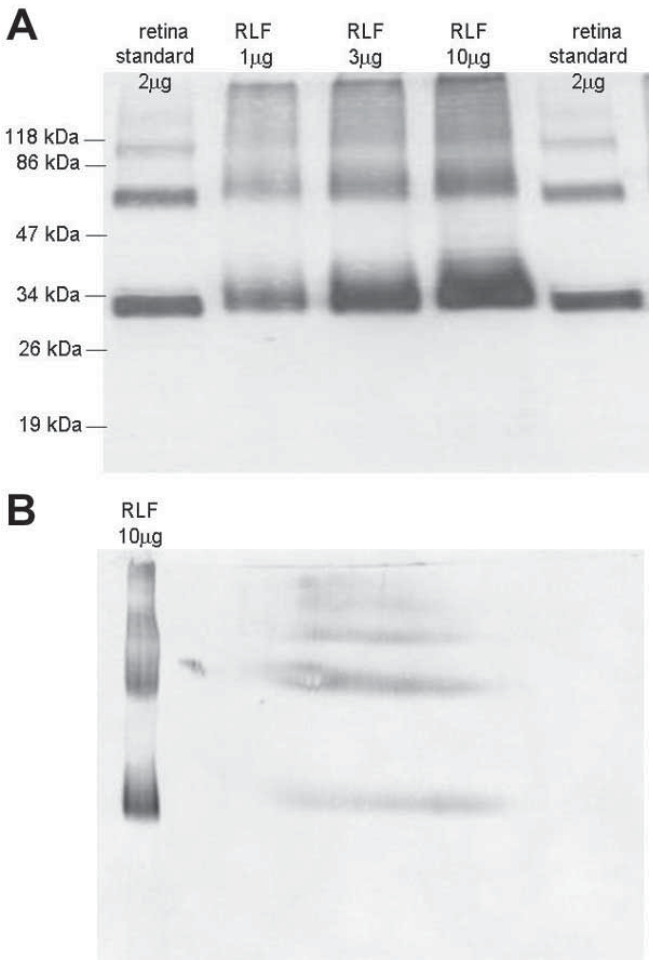

Figure 6. Rhodopsin immunoblots of RLF. **A**: Immunoblot following SDS-PAGE of 1, 3, and 10 μg of total RLF protein. Shown for comparison is 2 μg of protein from photoreceptor cell membranes enriched from human retina. Rhodopsin runs on SDS-PAGE as a mixture of the monomer (about 30 kDa), dimer (about 60 kDa), and trimer (about 90 kDa). **B**: Immunoblot following 2D electrophoresis of 10 μg of total RLF protein. For comparison, 10 μg of RLF protein was loaded in the standards lane of the second dimension gel. The diffusion (band broadening, due to modifications) of the rhodopsin in RLF as compared with that in photoreceptor cells indicates that the rhodopsin in RLF is remarkably heterogeneous.

DISCUSSION

Detecting membrane and microheterogeneous proteins: We report the identification of proteins in retinal lipofuscin (RLF) granules. Because of the lipophilic nature of RLF granules and the apparent inability of RPE cells to degrade them, one would expect to find an abundance of hydrophobic and highly modified, microheterogenous proteins in RLF granules. Due to the limitations of 2D electrophoresis, including the lack of solubility of hydrophobic proteins in buffer systems compatible with 2D electrophoresis and the inability to focus microheterogeneous proteins into observable spots, 1D electrophoresis was also used to identify proteins in RLF. The previous report [11] employed only 2D electrophoresis, which limited the proteins amenable to identification. We have identified 41 total proteins, only five of which were found in both

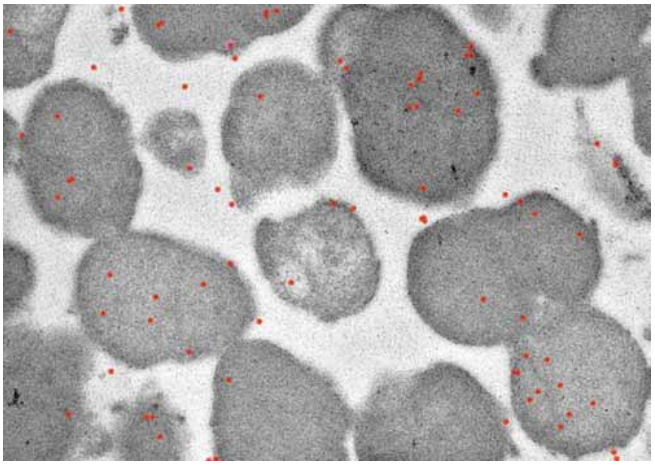

Figure 7. Immunocytochemistry of RLF. RLF granules were fixed and embedded in resin. Thin sections were collected on gold grids, incubated with an anti-rhodopsin antibody, washed, incubated with gold-conjugated protein A, washed, and examined using transmission electron microscopy (TEM). TEM showed gold-conjugated protein A bound to anti-rhodopsin antibodies on the RLF granules as dark black dots, which have been pseudocolored red. Rhodopsin is an integral part of the RLF granules.

1D and 2D gels. Of the 41 proteins that we identified and the 65 nonredundant proteins identified by Schutt et al. [11], only 12 (11%) were common to both studies.

An aspect influencing the discrepancy between protein identifications from the two types of gels is the ability to detect highly hydrophobic proteins, which we expected to be abundant in RLF granules. We found 17 integral membrane and membrane-associated proteins (about 50% of all RLF-specific proteins we identified). The previous report of RLF proteins [11], which used 2D electrophoresis, found fewer membrane proteins. Of the 17 membrane associated proteins that we identified, 13 were found exclusively in our 1D gel slices, again testifying to the limitations of 2D electrophoresis in analyzing lipophilic proteins.

Another cause of the inconsistency in proteins identified from 1D and 2D gels may be from contaminants of RLF preparations. Contaminants of RLF preparations are likely to be greatly exacerbated in 2D electrophoresis because they might run as well focused spots, whereas many of the authentic RLF proteins are microheterogeneous and therefore do not focus on 2D gels (rhodopsin being a notable example, Figure 6). Whenever preparations of subcellular structures are made using centrifugation for separation based on density, some contamination is inevitable. Indeed, as several others have noted, such preparations are not truly purifications but are enrichments [23]. While these are nonetheless valuable preparations, caution should be exercised in drawing conclusions when analyzing them. We found that we had to load significantly more material onto the 2D gels than we would have expected for an enriched subcellular granule. This may have resulted in an overloading of the focusable protein contaminants, such that they became visible as spots that were subsequently identified (CRALBP as an example, Figure 8). For this reason, we also employed complementary protein identification from 1D gels. We are aware that the methods we have used do not identify every protein in the preparations we have studied. Attempting to exhaustively identify all of the proteins in an enriched

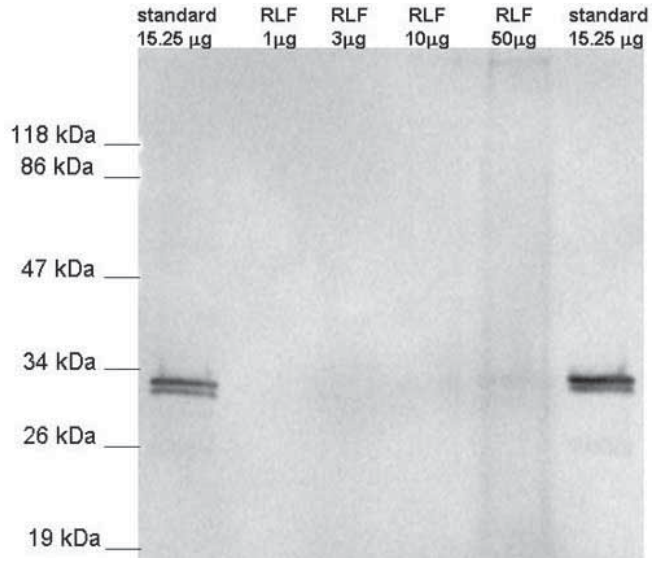

Figure 8. CRALBP immunoblot of RLF. Doses of 1, 3, 10, and 50 µg total RLF protein were run on SDS-PAGE and blotted with an anti-CRALBP antibody. Shown for comparison are 15.25 µg of total protein extracted from human RPE. CRALBP is nearly absent from RLF.

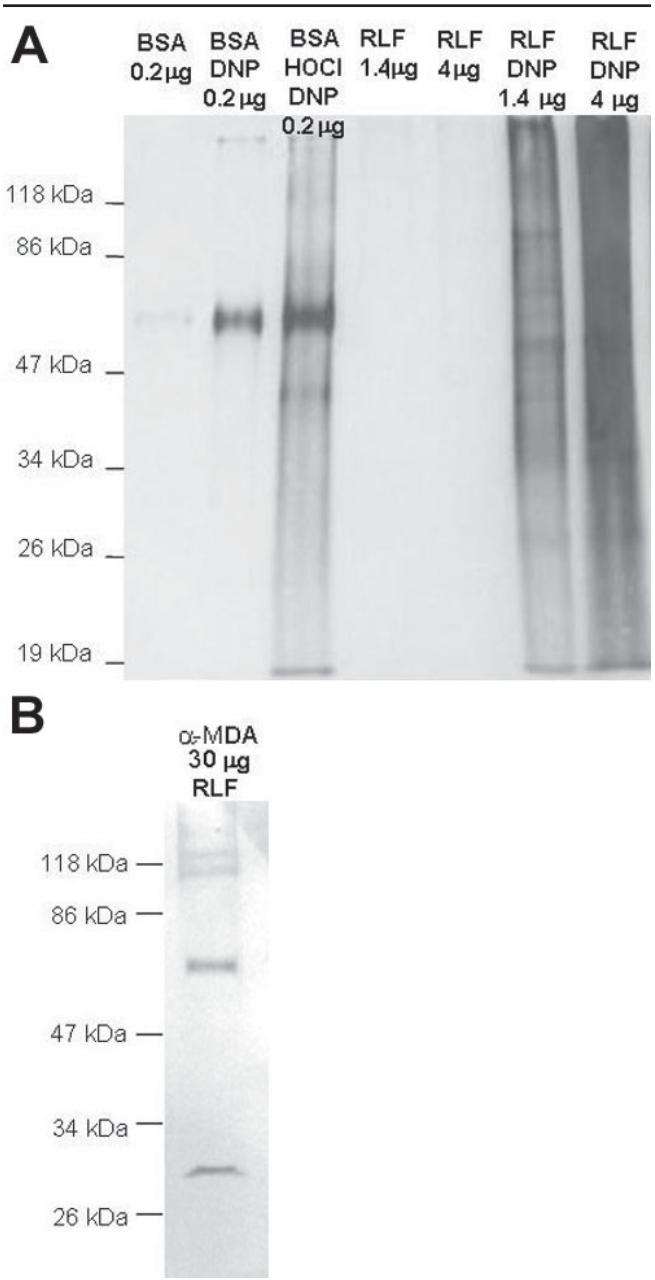

Figure 9. Immunoblots of oxidatively damaged RLF proteins. **A**: RLF proteins, 1.4 and 4 µg, that had been derivatized with dinitrophenyl hydrazine (right two lanes) or that were untreated (middle two lanes) were run on SDS-PAGE and blotted with an anti-DNP antibody to show the derivatized protein carbonyls, a common product of protein oxidative damage. Shown for comparison and to demonstrate specificity are lanes of BSA, BSA treated with DNPH, and BSA oxidized with hypochlorite then treated with DNPH. **B**: 30 and 150 µg of RLF proteins were separated using SDS-PAGE and blotted with an anti-MDA antibody to show RLF proteins containing lipid peroxidation-induced damage. There is extensive oxidative damage to RLF proteins.

preparation such as lipofuscin granules would be misleading because many contaminating proteins would be identified. Nonetheless, the proteins we have identified give us a useful, even if somewhat incomplete, view of the protein constituents of RLF.

We have shown that these granules exhibit the fluorescence characteristics and microscopic structure previously reported [12]. We also show that the granules that we have isolated and characterized physically are biologically active, causing blue-light-dependent cell death to RPE cells in culture (Figure 1), as others have previously reported [5]. The only physical characterization of the granules offered by Schutt et al. [11] of their RLF preparation was fluorescence spectroscopy. As shown in Figure 3, the excitation and particularly the emission spectra reported by these authors were significantly dissimilar from our fluorescence spectra and from spectra previously reported in the literature.

Identifying phagosomal, lysosomal, and photoreceptor proteins: Our protein identifications are supportive of the hypothesis that RLF has a lysosomal/phagosomal origin. Four proteins that are lysosomal in subcellular localization were found in our RLF preparations. The proteome of macrophage phagosomes has recently been published [24], and 10 of the 41 proteins in our RLF preparations, which presumably have a phagosomal origin, are shared with the phagosomal proteome as reported [24].

The prevailing model of RLF origin is that there is a breakdown in the lysosomal machinery responsible for the degradation of the photoreceptor outer segments that are phagocytosed diurnally by the RPE, leading to an accumulation of indigestible material that becomes RLF. Our protein identifications strongly support such a model. Six of the RLF proteins that we identified are specific to photoreceptors and their outer segments. Only one of these was previously reported as a constituent of RLF [11].

Identifying rhodopsin: One of the most significant proteins that we observed in RLF, not observed previously, is rhodopsin, one of the most abundant proteins of photoreceptor outer segments. We did not observe rhodopsin among our 2D gel spots. Immunoblotting of our 2D gels showed that this was due to the lack of focusing of the microheterogeneous rhodopsin population in RLF (Figure 6). It is significant that the rhodopsin observed is rather extensively modified, at least in part due to oxidative damage. Though we were not able to quantify RLF rhodopsin precisely, our immunoblot evidence suggests that this protein is fairly abundant in RLF. Although Feeney-Burns et al. [25] were unable to observe rhodopsin in RLF granules, we believe that this was due to the antibody they used. As shown in Figure 7 our anti-rhodopsin antibody (R4) specifically bound to RLF granules confirming that the rhodopsin observed is a component of the granules and not merely a contaminant. The opsin we identified was exclusively rhodopsin, and no evidence was found that cone opsins were present in RLF. It has been previously noted that the cone-rich fovea is not as high in RLF as the rest of the macula [26].

Other specific proteins of interest: Two RLF proteins of interest, found in both 1D and 2D gels, are the ceroid lipofuscinosis protein and cathepsin D. Ceroid lipofuscinosis proteins are found to be mutated in Batten's disease, a condition in which there is significant accumulation of lipofuscin in neuronal tissue [27]. The ceroid lipofuscinosis proteins accumulate in the lipofuscin granules, along with ATP synthase, other proteins, and lipids [27,28]. Finding cathepsin D in RLF was not surprising. This lysosomal protease is highly expressed in RPE lysosomes, and is employed by these cells in degrading rhodopsin [29].

Another protein of interest in these studies is the cellular retinoid binding protein CRALBP, a protein sometimes used as a molecular marker for RPE cells (but also found in the Müller cells of the neural retina [30]). Schutt et al. [11] found CRALBP to be one of the most abundant proteins in their preparations (approximately the fifth most intense spot on the 2D gel, though two proteins were identified from this spot). In contrast, we find CRALBP to be the 69th most abundant of 121 spots in one gel, and absent from the other three 2D gels (data not shown). We did not identify CRALBP from our 1D gels, presumably because it was lost among more abundant proteins. As seen in Figure 8, immunoblotting shows that while CRALBP is present in gels of RLF, it is not very abundant. It is probable that CRALBP is a contaminant of these preparations.

Detecting protein modifications: A notable observation from this work is the nature and extent of modifications seen in RLF proteins. Derivatization using DNPH followed by immunoblot analyses with the anti-DNP antibody shows the presence of abundant protein carbonyl groups in RLF, indicating extensive oxidative damage to proteins. While protein carbonyls are diagnostic of oxidative damage to proteins [22,31], they are certainly not the only covalent modification that occurs to proteins as a result of such damage. Neither Met-sulfoxide nor Met-sulfone are derivatized with DNPH. A notable modification to proteins under oxidative stress is their fragmentation into smaller polypeptides by the breakage of backbone bonds [31]. Such damage would result in peptides upon trypsinization that have amino or carboxy termini that would not be predicted from the sequence databases, and may be further modified in terms of covalent structure. Additionally, covalent modifications of proteins due to oxidative damage are not yet completely understood, and many unknown modifications could be present, further complicating the proteomic analyses of the in-gel digest mass spectrometry data. Indeed, we observed a remarkably high fraction (about 75%) of our "good" CID spectra (criteria given in Results) that did not yield peptide identification, possibly because many of the peptides in question are modified in unknown ways. The only modification that we were able to identify precisely was oxidation of two methionine residues on rhodopsin, including the formation of the sulfone and the sulfoxide (Figure 5A). Ryan et al. [28] showed oxidation of methionine in ceroid lipofuscinosis protein in lipofuscin of neural tissue. We mention their findings, because we find the parallel between RLF and neural lipofuscin suggestive. We find that both the ceroid lipofuscinosis protein itself and methionine oxidation are found in RLF. Though we believe that there are significant differ-

ences between RLF and lipofuscin in other tissues such as neurons; we also believe that they are not wholly dissimilar. The facts that methionine oxidation is seen in both types of lipofuscin, and ceroid lipofuscinosis protein (a lysosomal component) occurs in both types suggests to us that oxidative protein damage inhibiting lysosomal function may be a shared characteristic (or even causal factor) in the two types of lipofuscin.

A previous report on RLF proteins [11] was followed up with an article showing immunological analyses of RLF proteins modified by hydroxynonenol (HNE), malonyldialdehyde (MDA), and advanced glycation end-products (AGE) [32]. Many of these modifications would be derivatized by DNPH, and thus would be part of the modified proteins that we observed in Figure 7A. For example, HNE has been shown to react with proteins resulting in a loss of sulfhydryls and a concomitant increase in DNPH reactivity [33]. In addition, 22% of the MDA incorporated into polylysine became aminopropenal, which has a DNPH-reactive aldehyde moiety [33]. Furthermore, one of the two aldehydes in MDA can react with a protein yielding the imine and possibly leave the other aldehyde to react with the hydrazine. Glycation, through a Maillard reaction, creates Amadori products that have free carbonyl groups [27]. The previous report [32] identified 32 2D gel spots that react with an anti-MDA antibody, 15 spots that react with an anti-HNE antibody, and four spots that react with an anti-AGE antibody. Notably, all of these are well-focused spots, as opposed to the heterogeneously modified proteins we observed with DNP derivatization (Figure 9A). We observed that an anti-MDA antibody reacted with only a handful of RLF proteins (Figure 9B), and that an anti-AGE antibody reacted weakly with a heterogeneous smear of proteins from RLF (data not shown). Thus, it is eminently possible that the general oxidative damage that we describe might well include specific modifications such as those resulting from MDA, HNE, and AGE. Our specific efforts to duplicate the findings of Schutt et al. [32] using our RLF preparations yielded different findings, suggesting the need for further study of the roles of these specific modifications in the biochemistry of RLF.

Much has yet to be learned about the modifications of proteins in RLF granules. Perhaps it is the oxidative modification of proteins (and possibly of lipids as well) that inhibits the degradative machinery of the RPE lysosomes, and leads to the accumulation of RLF within these cells. Protease inhibition causes lipofuscin formation in myocytes [34]. Oxidative stress causes accelerated lipofuscinogenesis in various cells, and there is a dramatic synergy between oxidative stress and inhibition of lysosomal proteases (allowing more time for oxidation) in lipofuscin formation in cultured cells [34]. Nilsson et al. [35] found greatly enhanced accumulation of RLF in RPE cells cultured in 40% ambient oxygen when compared with cells cultured in 8% ambient oxygen. We are pursuing experiments aimed at understanding the possible role of oxidative damage of proteins in lipofuscinogenesis and other aspects of RLF origins and activities.

ACKNOWLEDGEMENTS

We gratefully thank and acknowledge: Dr. Paul S. Bernstein for providing human RPE and retinal samples, Dr. Barry M. Willardson for providing the R4 antibody, Dr. John C. Saari for providing the anti-CRALBP antibody, Dr. Kim Howes for providing the anti-AGE antibody, Dr. Paul B. Savage for the use of the fluorometer, Dr. Nolan F. Mangelson for the use of the microbalance, the staff of the BYU Microscopy Lab for their assistance, the data analysis assistance of David Almond, Emily Palenske and Dr. Wilfred Tang, the advice of Drs. Matthew C. Asplund and Merritt B. Andrus, and the technical assistance of Wayne E. Davis and Dr. Zhibing Chen. SW was a recipient of the Stanley and Leona Goates Research Fellowship and a Roland K. Robins Graduate Research Fellowship. This research was supported by the Brigham Young University College of Physical and Mathematical Sciences and the Department of Chemistry and Biochemistry.

REFERENCES

1. Delori FC, Goger DG, Dorey CK. Age-related accumulation and spatial distribution of lipofuscin in RPE of normal subjects. Invest Ophthalmol Vis Sci 2001; 42:1855-66.
2. Mata NL, Weng J, Travis GH. Biosynthesis of a major lipofuscin fluorophore in mice and humans with ABCR-mediated retinal and macular degeneration. Proc Natl Acad Sci U S A 2000; 97:7154-9.
3. Feeney-Burns L, Hilderbrand ES, Eldridge S. Aging human RPE: morphometric analysis of macular, equatorial, and peripheral cells. Invest Ophthalmol Vis Sci 1984; 25:195-200.
4. Beatty S, Koh H, Phil M, Henson D, Boulton M. The role of oxidative stress in the pathogenesis of age-related macular degeneration. Surv Ophthalmol 2000; 45:115-34.
5. Winkler BS, Boulton ME, Gottsch JD, Sternberg P. Oxidative damage and age-related macular degeneration. Mol Vis 1999; 5:32.
6. Rozanowska M, Jarvis-Evans J, Korytowski W, Boulton ME, Burke JM, Sarna T. Blue light-induced reactivity of retinal age pigment. In vitro generation of oxygen-reactive species. J Biol Chem 1995; 270:18825-30.
7. Wassell J, Davies S, Bardsley W, Boulton M. The photoreactivity of the retinal age pigment lipofuscin. J Biol Chem 1999; 274:23828-32.
8. Feeney-Burns L, Eldred GE. The fate of the phagosome: conversion to 'age pigment' and impact in human retinal pigment epithelium. Trans Ophthalmol Soc U K 1983; 103:416-21.
9. Eldred GE, Katz ML. Fluorophores of the human retinal pigment epithelium: separation and spectral characterization. Exp Eye Res 1988; 47:71-86.
10. Eldred GE, Lasky MR. Retinal age pigments generated by self-assembling lysosomotropic detergents. Nature 1993; 361:724-6.
11. Schutt F, Ueberle B, Schnolzer M, Holz FG, Kopitz J. Proteome analysis of lipofuscin in human retinal pigment epithelial cells. FEBS Lett 2002; 528:217-21.
12. Boulton M, Docchio F, Dayhaw-Barker P, Ramponi R, Cubeddu R. Age-related changes in the morphology, absorption and fluorescence of melanosomes and lipofuscin granules of the retinal pigment epithelium. Vision Res 1990; 30:1291-303.
13. Verhaert P, Uttenweiler-Joseph S, de Vries M, Loboda A, Ens W, Standing KG. Matrix-assisted laser desorption/ionization quadrupole time-of-flight mass spectrometry: an elegant tool for peptidomics. Proteomics 2001; 1:118-31.

14. Shevchenko A, Wilm M, Vorm O, Mann M. Mass spectrometric sequencing of proteins silver-stained polyacrylamide gels. Anal Chem 1996; 68:850-8.
15. Takemoto DJ, Spooner B, Takemoto LJ. Antisera to synthetic peptides of bovine rhodopsin: use as site-specific probes of disc membrane changes in retinal dystrophic dogs. Biochem Biophys Res Commun 1985; 132:438-44.
16. Thulin CD, Howes K, Driscoll CD, Savage JR, Rand TA, Baehr W, Willardson BM. The immunolocalization and divergent roles of phosducin and phosducin-like protein in the retina. Mol Vis 1999; 5:40.
17. Shacter E, Williams JA, Lim M, Levine RL. Differential susceptibility of plasma proteins to oxidative modification: examination by western blot immunoassay. Free Radic Biol Med 1994; 17:429-37.
18. Sohal RS, Wolfe LS. Lipofuscin: characteristics and significance. Prog Brain Res 1986; 70:171-83.
19. Boulton M, Marshall J, Wong HC. The generation of dense granules within cultured human retinal pigment epithelial cells at senescence. Graefes Arch Clin Exp Ophthalmol 1986; 224:106-9.
20. Santoni V, Vinh J, Pflieger D, Sommerer N, Maurel C. A proteomic study reveals novel insights into the diversity of aquaporin forms expressed in the plasma membrane of plant roots. Biochem J 2003; 373:289-96.
21. Schlunck G, Martin G, Agostini HT, Camatta G, Hansen LL. Cultivation of retinal pigment epithelial cells from human choroidal neovascular membranes in age related macular degeneration. Exp Eye Res 2002; 74:571-6.
22. Shacter E. Protein oxidative damage. Methods Enzymol 2000; 319:428-36.
23. Brunet S, Thibault P, Gagnon E, Kearney P, Bergeron JJ, Desjardins M. Organelle proteomics: looking at less to see more. Trends Cell Biol 2003; 13:629-38.
24. Garin J, Diez R, Kieffer S, Dermine JF, Duclos S, Gagnon E, Sadoul R, Rondeau C, Desjardins M. The phagosome proteome: insight into phagosome functions. J Cell Biol 2001; 152:165-80.
25. Feeney-Burns L, Gao CL, Berman ER. The fate of immunoreactive opsin following phagocytosis by pigment epithelium in human and monkey retinas. Invest Ophthalmol Vis Sci 1988; 29:708-19.
26. Sparrow, J. R., Cai, B., Fishkin, N., Jang, Y. P., Krane, S., Vollmer, H., Zhou, J., and Nakanishi, K. A2E, a fluorphore of RPE lipofuscin: Can it cause RPE degeneration? In: LaVail MM, Hollyfield JG, Anderson RE, editors. Retinal degenerations: mechanisms and experimental therapy. Proceedings of the 10th International Symposium on Retinal Degenerations; 2002 Sep 30-Oct 5; Burgenstock, Switzerland. New York: Kluwer Academic/Plenum; 2003. p. 205-11.
27. Yin D. Biochemical basis of lipofuscin, ceroid, and age pigment-like fluorophores. Free Radic Biol Med 1996; 21:871-88.
28. Ryan EM, Buzy A, Griffiths DE, Jennings KR, Palmer DN. Electrospray ionisation mass spectrometry (ESI/MS) of ceroid lipofuscin protein; a model system for the study of F0 inhibitor interactions with mitochondrial subunit C. Biochem Soc Trans 1996; 24:289S.
29. Zimmerman WF, Godchaux W 3rd, Belkin M. The relative proportions of lysosomal enzyme activities in bovine retinal pigment epithelium. Exp Eye Res 1983; 36:151-8.
30. Johnson PT, Geller SF, Lewis GP, Reese BE. Cellular retinaldehyde binding protein in developing retinal astrocytes. Exp Eye Res 1997; 64:759-66.
31. Berlett BS, Stadtman ER. Protein oxidation in aging, disease, and oxidative stress. J Biol Chem 1997; 272:20313-6.
32. Schutt F, Bergmann M, Holz FG, Kopitz J. Proteins modified by malondialdehyde, 4-hydroxynonenal, or advanced glycation end products in lipofuscin of human retinal pigment epithelium. Invest Ophthalmol Vis Sci 2003; 44:3663-8.
33. Esterbauer H, Schaur RJ, Zollner H. Chemistry and biochemistry of 4-hydroxynonenal, malonaldehyde and related aldehydes. Free Radic Biol Med 1991; 11:81-128.
34. Brunk UT, Terman A. Lipofuscin: mechanisms of age-related accumulation and influence on cell function. Free Radic Biol Med 2002; 33:611-9.
35. Nilsson SE, Sundelin SP, Wihlmark U, Brunk UT. Aging of cultured retinal pigment epithelial cells: oxidative reactions, lipofuscin formation and blue light damage. Doc Ophthalmol 2003; 106:13-6.

The print version of this article was created on 15 Dec 2005. This reflects all typographical corrections and errata to the article through that date. Details of any changes may be found in the online version of the article.